Multi-Task Learning with User Preferences: Gradient Descent with Controlled Ascent in Pareto Optimization

Debabrata Mahapatra [1] **Vaibhav Rajan** [2]

Abstract

Multi-Task Learning (MTL) is a well established paradigm for jointly learning models for multiple correlated tasks. Often the tasks conflict, requiring trade-offs between them during optimization. In such cases, multi-objective optimization based MTL methods can be used to find one or more Pareto optimal solutions. A common requirement in MTL applications, that cannot be addressed by these methods, is to find a solution satisfying user-specified preferences with respect to task-specific losses. We advance the state-of-the-art by developing the first gradient-based multi-objective MTL algorithm to solve this problem. Our unique approach combines multiple gradient descent with carefully controlled ascent to traverse the Pareto front in a principled manner, which also makes it robust to initialization. The scalability of our algorithm enables its use in large-scale deep networks for MTL. Assuming only differentiability of the task-specific loss functions, we provide theoretical guarantees for convergence. Our experiments show that our algorithm outperforms the best competing methods on benchmark datasets.

1. Introduction

Multi-Task Learning (MTL) is a paradigm where data for multiple related tasks is used to learn models for all the tasks simultaneously. It aims to improve over learning each task independently by utilizing the shared signal in the data through an inductive transfer mechanism (Caruana, 1997). Deep architectures based on MTL have led to state-of-the-art models in many areas, such as computer vision (Liu et al., 2019a), natural language processing (Liu et al., 2019b) and bioinformatics (Ramsundar et al., 2015).

A common approach to train MTL models is by minimizing the weighted sum of the empirical losses for each task, also known as the *linear scalarization* approach. However, this formulation cannot model competing tasks that arise in many real-world applications, e.g., during drug design we may want to simultaneously increase drug effectiveness and decrease development cost. It may not be possible to optimize all the objectives simultaneously and trade-offs between tasks may be required. In such cases, *Pareto optimal* solutions, obtained through multi-objective optimization, are natural choices where each optimal solution is non-dominated, i.e., no objective value can be improved further without degrading some other objectives. There can be multiple (possibly infinite) Pareto optimal solutions, represented by the *Pareto front*, each solution with a different trade-off between the conflicting objectives.

The efficacy of multi-objective optimization for MTL was first shown by Sener & Koltun (2018). Their algorithm extends the Multiple Gradient Descent Algorithm (Désidéri, 2012) to handle high-dimensional gradients, thereby making it suitable for large-scale MTL with deep networks. However, their method finds a single arbitrary solution from the Pareto set and cannot be used by MTL designers to explore solutions with different trade-offs. This limitation was recognized by Lin et al. (2019) who partly address this problem by decomposing the MTL problem and solving multiple subproblems with different trade-offs. Their method yields a set of Pareto optimal solutions distributed over the Pareto front.

In many MTL applications, the designer may want to explore solutions with *specific* trade-offs in the form of preferences or priorities among the tasks. For instance, in multi-task recommender systems (Milojkovic et al., 2019) which optimizes semantic relevance, content quality and revenue, one may want (one or more) solutions that prioritizes relevance over quality. Similar requirements arise in, e.g., emotion recognition (Zhang et al., 2017) and the autonomous driving self-localization problem (Wang et al., 2018). Formally, given preferences r_j for each task, a Pareto optimal solution is required such that for any two tasks, if $r_i \geqslant r_j$,

[1]Department of Computer Science, National University of Singapore [2]Department of Information Systems and Analytics, National University of Singapore. Correspondence to: Debabrata Mahapatra <debabrata@u.nus.edu>, Vaibhav Rajan <vaibhav.rajan@nus.edu.sg>.

Proceedings of the 37^{th} International Conference on Machine Learning, Online, PMLR 119, 2020.

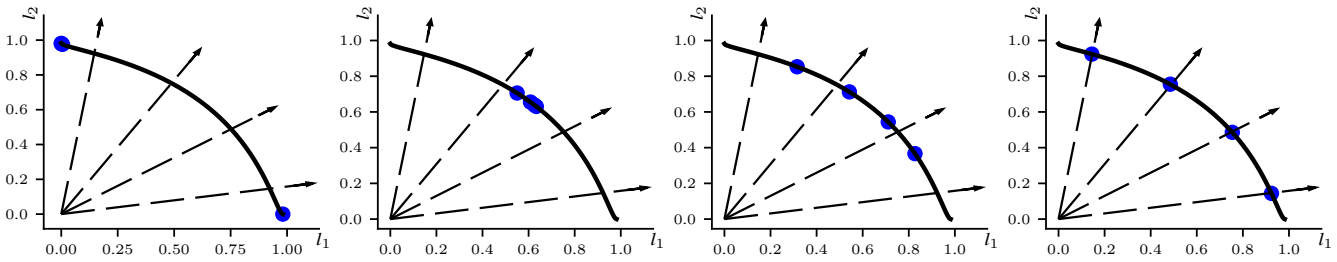

(a) Linear Scalarization (b) MGDA (c) Pareto MTL (d) EPO Search

Figure 1. (Color Online) Pareto front (solid curve) for two loss functions l_1, l_2 and solutions on the Pareto front (blue circles) for different preferences (dashed rays) obtained by (a) Linear Scalarization: cannot find solutions in the concave part; (b) MGDA-based methods (e.g., (Sener & Koltun, 2018)): finds arbitrary Pareto optimal solutions (does not use input preference vectors); (c) Pareto MTL (Lin et al., 2019): divides the Pareto front using multiple reference vectors to find solutions in the sub-regions; (d) EPO Search: can find exact solutions at any given preference vector. See section 3.2 for more details and section 5.1 for experiment settings.

then the corresponding losses follow $l_i \leqslant l_j$. We call such a solution a **preference-specific** Pareto optimal solution.

Finding preference-specific Pareto optimal solutions is challenging and cannot be solved by either linear scalarization or existing multi-objective MTL methods. A preference vector determines a direction and hence a point on the Pareto front. Current methods cannot be used to reach a specific point on the Pareto front (see fig. 1 and section 3.2). We advance the state-of-the-art in multi-objective MTL methods by solving this problem. Our contributions in this paper are:

- We develop the first gradient-based multi-objective MTL algorithm, called Exact Pareto Optimal (EPO) Search, to find a preference-specific Pareto optimal solution[1].
- The unique approach of EPO Search combines gradient descent and carefully controlled ascent, enabling it to:
  - traverse the Pareto front until the required solution is reached, thereby making it robust to initialization.
  - find a Pareto optimal solution closest to the preference if an exact solution does not exist.
  - find multiple exact solutions on the Pareto front in a principled manner, if multiple preferences are given.
  - scale linearly with the gradient dimension and thereby efficiently train large-scale deep networks for MTL.
- Assuming only differentiability of loss functions (they need not be convex), we prove that EPO Search converges to the exact preference-specific Pareto optimal.
- Experiments on synthetic and real data demonstrate the superiority of EPO Search over state-of-the-art methods.

2. Related Work

MTL has been studied extensively – see (Zhang & Yang, 2018) for a general survey and (Ruder, 2017) for a survey of neural MTL models. The most common neural approach is to learn shared representations from data of related tasks, and optimization typically involves linear scalarization and its variants, such as those with adaptive weights (Chen et al., 2018; Heydari et al., 2019). Competing tasks and the trade-offs between them cannot be modeled by such methods.

The problem of simultaneously optimizing multiple, possibly conflicting criteria has been studied in Multiobjective Optimization (MOO). Excellent surveys can be found in (Marler & Arora, 2004; Gandibleux, 2006; Deb, 2014; Wiecek et al., 2016). Gradient-free approaches are commonly used in MOO solvers (e.g., evolutionary algorithms (Deb, 2001; Coello, 2006), continuation methods (Schütze et al., 2005; Ringkamp et al., 2012) and deterministic approaches (Ehrgott, 2005; Evtushenko & Posypkin, 2014)). In comparison, gradient-based approaches (Fliege & Svaiter, 2000; Fliege et al., 2009; Désidéri, 2012; Fliege & Vaz, 2016; Peitz & Dellnitz, 2018) are computationally less intensive (Zerbinati et al., 2011).

Various kinds of preferences, such as objective weights, goal specification and desirability thresholds, can be incorporated in a MOO, as surveyed in (Rachmawati & Srinivasan, 2006; Bechikh et al., 2015). Reference point or weight vector based methods that can model priorities between criteria, e.g., (Deb & Sundar, 2006; Cheng et al., 2016), typically find regions in the Pareto front close to the given references. The weighted Tchebycheff method (Steuer, 1989) and its variants (see Wiecek et al. (2016) for a survey), formulate a single objective optimization (SOO) problem using the given objective function weights. Although its solution can be preference-specific for some weights, this method cannot explore the Pareto Front for all trade-off combinations (Miettinen, 1998). To our knowledge, no previous gradient-based MOO algorithm can find an exact preference-specific Pareto optimal solution.

Pareto optimal solutions with different trade-offs were first modeled in MTL through gradient-based MOO by Sener & Koltun (2018). Their approach was generalized by Lin et al. (2019) whose method yields multiple Pareto optimal

[1]Python implementation available at: `https://github.com/dbmptr/EPOSearch`

solutions with different trade-offs. This work is closest to ours and we give a technical description in section 3.2.

3. Preliminaries

We consider m tasks, each with a non-negative objective function, $l_j : \mathbb{R}^n \to \mathbb{R}_+, j \in [m]$. The vector valued function $l : \mathbb{R}^n \to \mathbb{R}^m$ is a mapping from the *Solution space* $\mathbb{R}^n$ to the *Objective space* $\mathbb{R}^m$. We use l to denote both the loss function and a point in $\mathbb{R}^m$, which should be clear from the context. The range of l, denoted by $\mathcal{O}$, is a subset of the positive cone:

$$\mathbb{R}^m_+ := \{l \in \mathbb{R}^m \mid l_j \geqslant 0 \; \forall j \in [m]\}. \tag{1}$$

The partial ordering for any two points $l^1, l^2 \in \mathbb{R}^m$, denoted by $l^1 \geqslant l^2$ is defined by $l^1 - l^2 \in \mathbb{R}^m_+$, which implies $l^1_j \geqslant l^2_j$ for every $j \in [m]$ and strict inequality $l^1 > l^2$ occurs when there is at least one j for which $l^1_j > l^2_j$. Geometrically, $l^1 > l^2$ means that l^1 lies in the positive cone pivoted at l^2, i.e. $l^1 \in \{l^2\} + \mathbb{R}^m_+ := \left\{l^2 + l \;\middle|\; l \in \mathbb{R}^m_+\right\}$, and $l^1 \neq l^2$.

In the context of minimization, a solution $\theta^1 \in \mathbb{R}^n$ is *dominated* by another solution $\theta^2 \in \mathbb{R}^n$ iff $l(\theta^1) \geqslant l(\theta^2)$. Note that $l(\theta^1) \not> l(\theta^2)$ if θ^1 is not dominated by θ^2, i.e. $l(\theta^1) \notin \{l(\theta^2)\} + \mathbb{R}^m_+$. A solution θ^* is **Pareto optimal** if it is not dominated by any other solution. The set of all global Pareto optimal solutions is given by

$$\mathcal{P}_{glo} := \{\theta^* \in \mathbb{R}^n \mid \forall \theta \in \mathbb{R}^n - \{\theta^*\},\; l(\theta^*) \not> l(\theta)\}. \tag{2}$$

We are interested in local Pareto optimal solutions given by

$$\mathcal{P} := \left\{ \theta^* \in \mathbb{R}^n \;\middle|\; \begin{array}{l} \exists\, \mathcal{N}(\theta^*) \subset \mathbb{R}^n \mid \\ \forall \theta \in \mathcal{N}(\theta^*) - \{\theta^*\}, \\ l(\theta^*) \not> l(\theta) \end{array} \right\}, \tag{3}$$

where $\mathcal{N}(\theta^*)$ is an open neighbourhood of θ^*. Note that $\mathcal{P}_{glo} \subset \mathcal{P}$. The set of multi-objective values of the Pareto optimal solutions, $l(\mathcal{P}) \subset \mathcal{O}$, is called the **Pareto front**.

3.1. Gradient-based Multi-Objective Optimization

In gradient-based MOO, we find a Pareto optimal solution by starting from an arbitrary initialization $\theta^0 \in \mathbb{R}^n$ and iteratively finding the next solution θ^{t+1} that dominates the previous one θ^t (i.e., $l^{t+1} \preccurlyeq l^t$, where $l^t := l(\theta^t)$), by moving against a direction d with step size η, i.e. $\theta^{t+1} = \theta^t - \eta d$, such that descent happens in every objective, $l^{t+1}_j \leqslant l^t_j$. This can happen only if d has positive angles with the gradients of every objective function at θ^t.

Let $g_j = \nabla_\theta l_j$ be the gradient of the j^{th} objective function at θ, and $G \in \mathbb{R}^{n \times m}$ be the matrix having g_j as its j^{th} column. The **descent direction** d_{des} is given by $d^T_{des} g_j \geqslant 0$ for all $j \in [m]$. Thus, moving *against* d_{des}, starting from θ, amounts to a decrease in the objective values, with no change when $d^T_{des} g_j = 0$.

Désidéri (2012) showed that descent directions can be found in the *Convex Hull* of the gradients, defined by

$$\mathcal{CH}_\theta := \{G\beta \mid \beta \in \mathcal{S}^m\}, \tag{4}$$

$$\text{where } \mathcal{S}^m := \left\{\beta \in \mathbb{R}^m_+ \;\middle|\; \textstyle\sum_{j=1}^m \beta_j = 1\right\} \tag{5}$$

is the $m-$dimensional regular simplex, and their Multiple Gradient Descent Algorithm (MGDA) converges to a local Pareto optimal by iteratively using the descent direction

$$d^* = \arg\min_{d \in \mathcal{CH}_\theta} \|d\|_2^2. \tag{6}$$

Sener & Koltun (2018) design a method to solve (6) that scales to high-dimensional gradients.

3.2. Problem Statement

Given relative preferences for each task $r_j > 0, j \in [m]$, we want to find a Pareto optimal solution $\theta^*_r \in \mathcal{P}$ such that, if $r_j \geqslant r_{j'}$ then $l_j(\theta^*_r) \leqslant l_{j'}(\theta^*_r)$.

Limitations of current methods. We briefly discuss possible approaches to solving this problem with existing MTL methods and their limitations. Consider linear scalarization that uses *single objective optimization* (SOO) where the preferences can be task-specific weights:

$$\theta^* = \arg\min_\theta \; s(\theta) = r^T l(\theta). \tag{7}$$

As discussed in (Boyd & Vandenberghe, 2004)[Ch 4.7], if $\mathcal{O}$ is non-convex in $\mathbb{R}^m$ then it may not be possible to find such a θ^*_r; and the desired θ^*_r can be found only if $\mathcal{O}$ is convex near $l(\theta^*_r)$ and initialization θ^0 to solve (7) is done to ensure that θ^0 is not far from θ^*_r.

In MGDA-based algorithms (e.g., (Sener & Koltun, 2018)), using d_{des} we can only find a solution that dominates the previous one, without any control over moving towards the preference. Thus, depending on the initialization θ^0, the algorithm may reach *any* local Pareto optimal. This has also been empirically verified by Lin et al. (2019).

The Pareto MTL (PMTL) algorithm by Lin et al. (2019) finds multiple solutions on the Pareto front. Their algorithm uses several reference vectors $u_k, k = 1, \ldots, K$ to partition the solution space into K sub-regions $\Omega_k := \left\{\theta \in \mathbb{R}^n \;\middle|\; u_k^T l(\theta) \geqslant u_{k'}^T l(\theta)\; \forall k' \neq k\right\}$ and then has two phases. In the first phase, starting from an initial point, they find a point $\theta^0_r \in \Omega_k$, such that the corresponding u_k is the preferred direction of optimal multi-objective value $l(\theta^*_r)$. In the second phase, they iteratively use d_{des} to reach a Pareto optimal $\theta^* \in \mathcal{P}$ that is close to θ^*_r to find $l(\theta^*) \in l(\mathcal{P}) \cap l(\Omega_k)$. However, their method does not guarantee that the outcome of second phase θ^* also lies in

Ω_k. Moreover, to reach a desired preference, they have to increase the number of u_k exponentially with increase in number of tasks m, making it practically infeasible. Thus, although their reference vectors can be based on user preferences, their method, by design, does not reach the exact preference but only in the sub-regions of the Pareto front between the references (see fig. 1).

4. Exact Pareto Optimal Search

An **Exact Pareto optimal** (EPO) solution with respect to a preference vector r belongs to the set:

$$\mathcal{P}_r = \left\{\theta^* \in \mathcal{P} \;\middle|\; r_1 l_1^* = \cdots = r_j l_j^* = \cdots = r_m l_m^*\right\}, \quad (8)$$

where $l_j^* = l_j(\theta^*)$. Note that for any EPO solution θ_r^*, $l(\theta_r^*)$ is a point on the Pareto front intersecting the ray towards $r^{-1} := (1/r_1, \cdots, 1/r_m)$ (see fig. 1(d)) and $r \odot l$ is proportional to $\mathbf{1} = (1, \cdots, 1) \in \mathbb{R}^m$, where $\odot$ is the element-wise product operator. Clearly any EPO solution is a preference-specific Pareto optimal solution. We now develop our algorithm to find EPO solutions. Detailed proofs of all the theoretical results are in Appendix A.

To find EPO solutions, we not only have to find descent directions towards the Pareto front but also towards solutions that satisfy the condition in (8). To achieve the latter, we define a new criterion. For any point θ in the solution space $\mathbb{R}^n$, we define the **Non-Uniformity** of its objective values with respect to a given preference vector r as

$$\mu_r(l(\theta)) = \sum_{j=1}^{m} \hat{l}_j(\theta) \log\left(\frac{\hat{l}_j(\theta)}{1/m}\right), \quad (9)$$

$$= \mathrm{KL}\left(\hat{l}(\theta) \;\middle|\; \frac{\mathbf{1}}{m}\right), \quad (10)$$

where $\hat{l}_j$ is the weighted normalization

$$\hat{l}_j = \frac{r_j l_j}{\sum_{j'=1}^{m} r_{j'} l_{j'}}. \quad (11)$$

KL divergence of $\hat{l}$ from the uniform $\mathbf{1}/m$ befits the description of non-uniformity as it quantifies the extent to which $r_j l_j$ are unequal from each other: $\mu_r(l) = 0$ when all the $r_j l_j$ are equal, otherwise it is strictly positive. Moreover, the weighted normalized vector $\hat{l}$ always lies in $\mathcal{S}^m$. Fig. 2 plots μ_r for 3 objective functions and a preference vector.

4.1. Achieving Uniformity

We first find a direction such that if we move against it, starting from θ, then the non-uniformity of the new solution is less than that of θ. We use a linear combination of the m known gradients $g_j \in \mathbb{R}^n$ to construct the required

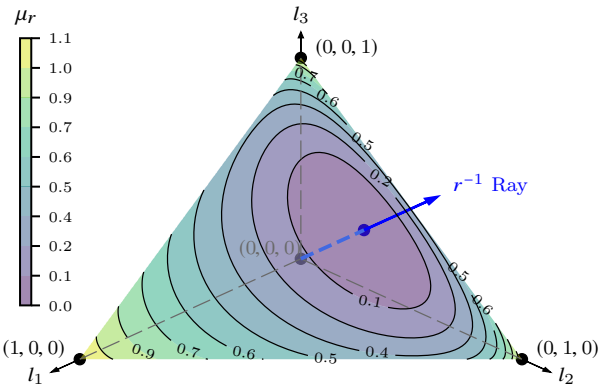

Figure 2. (Color Online) Variation of non-uniformity μ_r on the 3d simplex $\mathcal{S}^3$, for a specific preference vector $r = [0.6, 0.2, 0.2]$. The view is from $(1, 1, 1)$ direction towards origin.

"balancing" direction:

$$d_{bal} = \sum_{j=1}^{m} g_j a_j \quad (12)$$

where the weights a_j are the corresponding relative deviations from overall non-uniformity $\mu_r(l)$, that we call *adjustments*:

$$a_j = r_j \left(\log\left(\frac{\hat{l}_j}{1/m}\right) - \mu_r(l)\right). \quad (13)$$

We prove that d_{bal} guarantees decrease in non-uniformity.

Theorem 1. *If all the objective functions are differentiable, then for any direction $d \in \mathbb{R}^n$ with $d^T d_{bal} > 0$, there exists a step size $\eta_0 > 0$, such that*

$$\mu_r(l(\theta - \eta d)) \leqslant \mu_r(l(\theta)), \quad \forall \eta \in [0, \eta_0]. \quad (14)$$

Proof Sketch. A first order Taylor expansion of the multi-objective loss $l(\theta - \eta d)$ is used to lower bound $\mu_r(l(\theta)) - \mu_r(l(\theta - \eta d))$. We then show that this lower bound is positive if $d^T d_{bal} > 0$.

Notice that the adjustments a_j are non-negative for some objectives and negative for the rest, i.e., unless all $r_j l_j$ are equal, there will always be some objectives whose gradient terms in d_{bal} are negative.

Let $J = \{j \mid g_j^T d_{bal} > 0\}$ be the index set of all gradients that lie in the positive half plane of d_{bal}, and $\bar{J} = [m] - J$ be the index set for the gradients in the negative half plane of d_{bal}. If we use d_{bal} to move to a new solution $\theta_\eta^{t+1} = \theta^t - \eta d_{bal}$, then for some step size $\eta_0 > 0$,

$$l_j(\theta_\eta^{t+1}) < l_j(\theta^t), \quad \forall j \in J, \quad (15a)$$

$$\text{and } l_j(\theta_\eta^{t+1}) \geqslant l_j(\theta^t), \quad \forall j \in \bar{J}, \quad (15b)$$

for any $\eta \in (0, \eta_0]$. Thus, when d_{bal} is used to update a point θ^t, gradient *descent* happens for objectives in J, whereas gradient *ascent* happens for the objectives in $\bar{J}$.

Apart from facilitating a balancing direction in the solution space $\mathbb{R}^n$, the adjustments a in (13) have interesting properties in the objective space $\mathbb{R}^m$ as well. If we construct m vectors in $\mathbb{R}^m$ by using the gradients as

$$c_j = G^T g_j, \quad \forall j \in [m], \tag{16}$$

then the index sets J and $\bar{J}$ can be rewritten as

$$J = \{j \mid a^T c_j > 0\} \text{ and } \bar{J} = \{j \mid a^T c_j \leqslant 0\}. \tag{17}$$

Note that the matrix $C = G^T G \in \mathbb{R}^{m \times m}$ with c_j as its columns is a symmetric matrix. Another remarkable property of a is its relation with the loss vector l:

Claim 1. *The adjustment vector a is perpendicular to the multi-objective vector l in the objective space $\mathbb{R}^m$*

$$a^T l = 0. \tag{18}$$

4.2. Achieving Uniformity *and* Pareto optimality

We now seek a direction that enables us to move from a solution θ^t to θ^{t+1} such that either θ^{t+1} dominates θ^t ($l^{t+1} \preccurlyeq l^t$) or has better uniformity ($\mu_r(l^{t+1}) \leqslant \mu_r(l^t)$) or both. In other words, θ^{t+1} is not dominated by θ^t ($l^{t+1} \not\succ l^t$). We solve this problem through linear programming (LP).

From (Désidéri, 2012), we know that a descent direction in $d \in \mathcal{CH}_{\theta^t}$, the convex hull of the gradients at θ^t, will be towards the Pareto front. From (4) and (5), $d = G\beta$, where $\beta \in \mathcal{S}^m$, the $m-$dimensional simplex. From Theorem 1, we know that moving against a direction which makes a positive angle with $d_{bal} = Ga$, will improve uniformity. Combining the two requirements, we want to find a direction in $\mathcal{CH}_{\theta^t}$ that has maximum angle with d_{bal}, i.e., we maximize

$$d^T d_{bal} = \beta^T G^T G a = \beta^T C a. \tag{19}$$

However, once uniformity is achieved, when $\mu_r(l^t) = 0$ or the multi-objective value of the current iteration lies on the r^{-1} ray, we can enter a "pure descent" mode. This is done by finding a direction in $\mathcal{CH}_{\theta^t}$ whose inner product with the sum of all gradients is maximum. Thus, we maximize

$$\sum_{j=1}^{m} d^T g_j = \beta^T G^T G \mathbf{1} = \beta^T C \mathbf{1}. \tag{20}$$

Together, (19) and (20) give us our objective function, (24a), where $\mathbb{1}_{\mu_r^t}$ is a scalar indicator for non-zero $\mu_r(l^t)$.

In the pure descent mode, i.e., while maximizing (20), we simply require the constraint of a descent direction:

$$d^T g_j = \beta^T G^T g_j = \beta^T c_j \geqslant 0, \ \forall j \in [m]. \tag{21}$$

Algorithm 1 Update Equations for EPO Search

Input: $\theta^t \in \mathbb{R}^n$, preference $r \in \mathbb{R}^m$, and step size η
Objective Values: $l_j^t = l_j(\theta^t), \quad j \in [m]$
Gradients: $g_j = \frac{\partial l_j}{\partial \theta}\Big|_{\theta^t}, \quad j \in [m]$,
$G = [g_1, \cdots, g_m]$, $c_j = G^T g_j$, $C = [c_1, \cdots, c_m]$.
Non-uniformity: $\mu_r(l^t)$ (using (9))
Loss adjustments: a (using (13))
Index Sets: $J, \bar{J}, J^*$ (using (17), (23))
Find β^* by solving LP (24)
Non-dominating direction: $d_{nd} = G\beta^*$
Output: $\theta^{t+1} = \theta^t - \eta d_{nd}$

The non-negative angle of d with each gradient ensures that all objective values decrease and θ^{t+1} dominates θ^t.

When maximizing (19), the angle made by d with some of the gradients g_j need to be negative, to allow ascent for objectives with low values of $r_j l_j^t$ and descent for the ones with high-values. From (15), we know that ascent can happen for all the objectives in $\bar{J}$ if $d_{bal} \in \mathcal{CH}_{\theta^t}$. When $d_{bal} \notin \mathcal{CH}_{\theta^t}$, we can allow the required d to have negative angles with the gradients of objectives in $\bar{J}$. Since $a^T c_j \leqslant 0$, we achieve this by modifying (21) to $\beta^T c_j \geqslant a^T c_j, \ \forall j \in \bar{J}$.

When d_{bal} does not make positive angles with any of the gradients, i.e. J is empty and $\bar{J} = [m]$, we should not allow negative angles between d and the gradients, to prevent ascending all the objectives values simultaneously. This can be ensured by using a scalar indicator $\mathbb{1}_J$ for a non-empty index set J and further modifying the constraint to:

$$\beta^T c_j \geqslant a^T c_j \, \mathbb{1}_J, \quad \forall j \in \bar{J} \tag{22}$$

Finally, this ascent must be controlled to prevent the objective values from diverging while improving the uniformity. This is done by choosing descent for the objectives in the index set J^*, for the maximum relative objective values in the t^{th} iteration, given by:

$$J^* = \left\{ j \;\middle|\; r_j l_j^t = \max_{j'} \left\{ r_{j'} l_{j'}^t \right\} \right\}. \tag{23}$$

The proof of Theorem 2 shows that this ensures controlled ascent and convergence. Altogether, the final non-dominating direction $d_{nd} = G\beta^*$ is obtained by solving the following $m-$dimensional LP:

$$\beta^* = \arg\max_{\beta \in \mathcal{S}^m} \ \beta^T C \left(a \, \mathbb{1}_{\mu_r^t} + \mathbf{1} \left(1 - \mathbb{1}_{\mu_r^t} \right) \right) \tag{24a}$$

$$\text{s.t.} \quad \beta^T c_j \geqslant a^T c_j \, \mathbb{1}_J, \quad \forall j \in \bar{J} - J^* \tag{24b}$$

$$\beta^T c_j \geqslant 0 \,, \qquad \forall j \in J^*, \tag{24c}$$

We omit superscripts in C, a and J that change in every iteration to avoid clutter.

In an iteration t, the LP in (24) either maximizes $\beta^T C a$ or $\beta^T C \mathbf{1}$, but not both. We prove that, when the latter is chosen the LP finds a descent direction:

Lemma 1. *If $\mu_r(l^t) = 0$, then the non-dominating direction d_{nd} becomes a descent direction, i.e.*

$$d_{nd}^T g_j \geqslant 0, \quad \forall j \in [m]. \tag{25}$$

When $\mu_r(l^t) > 0$, we require a non-dominating direction that can either balance $r \odot l^t$ or descend the multi-objective value l^t. The LP also ensures this property:

Lemma 2. *Let $\gamma^* = a^T C \beta^*$ be the maximum value of the LP problem* (24) *when $\mu_r(l^t) > 0$.*

$$\text{If } \gamma^* > 0, \text{ then } d_{nd}^T d_{bal} > 0. \tag{26}$$

$$\text{If } \gamma^* \leqslant 0, \text{ then } d_{nd}^T g_j \geqslant 0, \ \forall j \in [m]. \tag{27}$$

In case of (26), we know from Theorem 1 that by moving against d_{nd}, the non-uniformity of l^t can be decreased whereas, in case of (27), d_{nd} becomes a descent direction.

Algorithm 1 shows all the steps in each iteration.

4.3. Convergence

We prove the convergence of our algorithm in two steps. First we define an admissible set $\mathcal{A}_{l^t}^r \subset \mathbb{R}^m$ that contains potential $l^{t+1} = l(\theta^{t+1})$ values in an iteration. Then we prove that the sequence of sets $\{\mathcal{A}_{l^t}^r\}$ converges to $\mathcal{P}_r$, the set of exact Pareto optimal solutions, if it exists. To characterize the properties of θ^{t+1} obtained by moving against d_{nd}, we define some sets in $\mathbb{R}^m$ that are illustrated in fig. 3.

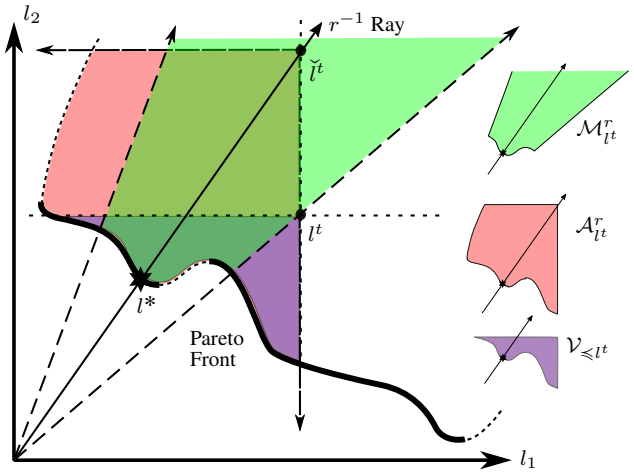

Figure 3. (Color Online) Illustration of the sets associated with the admissible set $\mathcal{A}_{l^t}^r$ in the objective space $\mathbb{R}^2$, at iteration t. This admissible set contains the multi-objective value l^{t+1} of next iteration.

The set of all attainable multi-objective values that dominate the current multi-objective l^t is denoted as

$$\mathcal{V}_{\preccurlyeq l^t} = \left\{ l \in \mathcal{O} \;\middle|\; l \preccurlyeq l^t \right\}. \tag{28}$$

The set of all attainable multi-objectives that have better uniformity than l^t is denoted as

$$\mathcal{M}_{l^t}^r = \{ l \in \mathcal{O} \mid \mu_r(l) \leqslant \mu_r(l^t) \}. \tag{29}$$

During descent $l^{t+1} \in \mathcal{V}_{\preccurlyeq l^t}$, and a balancing direction leads to $l^{t+1} \in \mathcal{M}_{l^t}^r$. For the t^{th} iteration, we define a point $\breve{l}^t \in \mathbb{R}_+^m$ as

$$\breve{l}^t = \lambda^t (1/r_1, \cdots, 1/r_m) \tag{30}$$

$$\text{where } \lambda^t = \max \{ l_j^t r_j \mid j \in [m] \}. \tag{31}$$

λ^t, and hence $\breve{l}^t$, are bounded, as each r_j is positive. Using $\breve{l}^t$ we define the admissible set as

$$\mathcal{A}_{l^t}^r = \left\{ l \in \mathcal{O} \;\middle|\; l \preccurlyeq \breve{l}^t \right\}, \tag{32}$$

which is also bounded. Note its relation with $\mathcal{V}_{\preccurlyeq l^t}$:

Lemma 3. *The set of dominating multi-objective points is a subset of the admissible set*

$$\mathcal{V}_{\preccurlyeq l^t} \subset \mathcal{A}_{l^t}^r. \tag{33}$$

Using lemmas 1, 2 and 3, we can show:

Theorem 2. *There exists a step size $\eta_0 > 0$, such that for every $\eta \in [0, \eta_0]$, the multi-objective value of the new solution point $\theta^{t+1} = \theta^t - \eta d_{nd}$ lies in the t^{th} admissible set*

$$l\left(\theta^{t+1}\right) \in \mathcal{A}_{l^t}^r. \tag{34}$$

Clearly, the admissible set contains all the points in $\mathcal{O}$ that dominate the l^t, i.e. $\mathcal{V}_{\preccurlyeq l^t} \subset \mathcal{A}_{l^t}^r$. Moreover, when $\mu_r(l^t) > 0$, it also has points with better uniformity than l^t, i.e. $\mathcal{A}_{l^t}^r \cap M_{l^t}^r \neq \phi$. Therefore, the admissible set contains the required solution for the next iteration, satisfying both uniformity and dominating properties. A natural consequence of Theorem 2 is the monotonicity of λ^t and $\mathcal{A}_{l^{t+1}}^r$.

Corollary 1. *The sequence of relative maximum values $\{\lambda^t\}$ is monotonic with $\lambda^{t+1} \leqslant \lambda^t$, which means*

$$\mathcal{A}_{l^{t+1}}^r \subset \mathcal{A}_{l^t}^r, \tag{35}$$

and the sequence of bounded sets $\{\mathcal{A}_{l^t}^r\}$ converges.

An interesting characteristic of λ^t is that if the non-uniformity $\mu_r(l^t) = 0$, then $l^t = \breve{l}^t$, hence $\mathcal{A}_{l^t}^r = \mathcal{V}_{\preccurlyeq l^t}$.

A Pareto solution is *regular* if its gradient matrix G has rank $m - 1$ (Zhang et al., 2008; Hillermeier, 2001). A necessary

condition for Pareto optimality is Pareto criticality (Fliege & Svaiter, 2000; Désidéri, 2012). At a Pareto critical point $\theta \in \mathbb{R}^n$ in the solution space, there exists a $\beta \in S^m$ such that $G\beta = 0 \in \mathbb{R}^n$. Previous gradient-based methods attain this condition at every Pareto optimal solution. In contrast, our proposed method is designed to find β, and hence meet the criticality condition, only at exact Pareto optimal solutions.

Claim 2. *Let $\theta^* \in \mathcal{P}$ be a regular Pareto optimal solution. If the set of exact Pareto optimal solutions $\mathcal{P}_r$ is nonempty, then the non-dominating direction $d_{nd} = G\beta^*$ found by the LP* (24) *is $0 \in \mathbb{R}^n$ if and only if $\theta^* \in \mathcal{P}_r$.*

Claim 2 shows that when an EPO solution exists, the algorithm does not stop prematurely at a local Pareto Optimal solution; it traces the Pareto front until an EPO solution is found. Beyond the mild regularity condition, this claim is true for certain irregular Pareto solutions as well (discussed in the proof). Note that if an EPO solution does not exist for the given r, our algorithm halts, i.e. d_{nd} becomes 0, at a Pareto optimal solution θ^* whose multi-objective value $l(\theta^*)$ has least non-uniformity $\mu_r(l(\theta^*))$ with respect r.

When a fixed step size is used for every iteration, the multi-objective values could fluctuate around the r^{-1} ray before converging to the EPO. To mitigate this problem we discuss modifications in our LP that lead to relaxed and restricted descent trajectories (see fig. 4) in Appendix B.

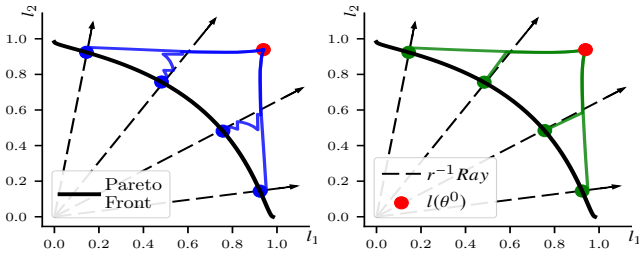

(a) Relaxed Descent (b) Restricted Descent

Figure 4. (Color Online) Modifications to our LP enable us to reduce and eliminate fluctuations in pure descent mode. See Appendix B for details.

4.4. Time Complexity

Our method scales linearly with the dimension (n) of the gradients, since the computation of $C = G^T G$ has runtime $O(m^2 n)$. With the current best LP solver (Cohen et al., 2019), our LP (24), that has m variables and at most $2m + 1$ constraints, has a runtime[2] of $O^*(m^{2.38})$. In deep MTL networks, usually $n \gg m$.

[2] O^* is used to hide $m^{o(1)}$ and $\log^{O(1)}(1/\delta)$ factors, δ being the relative accuracy. See (Cohen et al., 2019) for details.

5. Experiments

5.1. Synthetic Data

We illustrate the behavior of our algorithm using the synthetic data from (Lin et al., 2019). The two objectives to be minimized are non-convex functions:

$$l_1(\theta) = 1 - e^{-\left\|\theta - \frac{1}{\sqrt{n}}\right\|_2^2}, \tag{36a}$$

$$l_2(\theta) = 1 - e^{-\left\|\theta + \frac{1}{\sqrt{n}}\right\|_2^2}, \tag{36b}$$

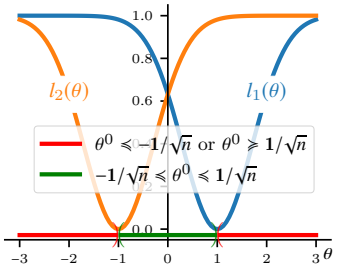

Figure 5. (Color Online) 1d solution space for (36)

where $\theta \in \mathbb{R}^n$, as shown in fig. 5. The set of attainable multi-objective values $\mathcal{O}$ is also non-convex in the objective space $\mathbb{R}^m$.

Note that linear scalarization misses any solution in the concave part of the Pareto front. The method of Sener & Koltun (2018) cannot use reference vectors (see fig. 1).

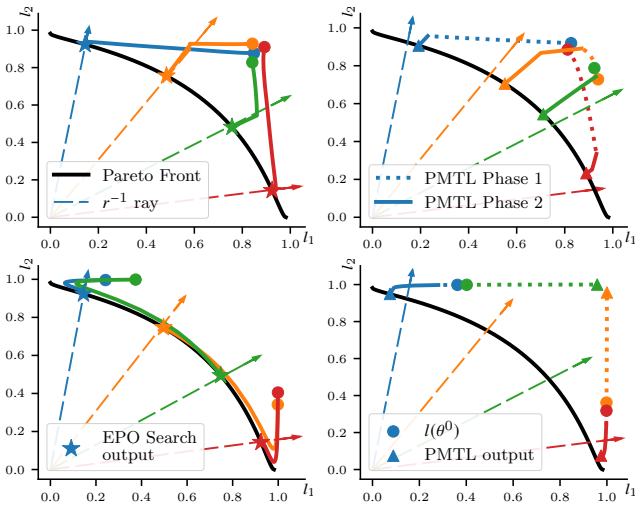

(a) EPO Search (b) Pareto MTL

Figure 6. (Color Online) Trajectories of EPO Search (left) and PMTL (right) in $\mathbb{R}^2$ with $n = 20$ dimensional solution space, when initializations are near Pareto optimal, $\theta^0 \in \mathcal{B}$ (Top) and are far, $\theta^0 \notin \mathcal{B}$ (Bottom).

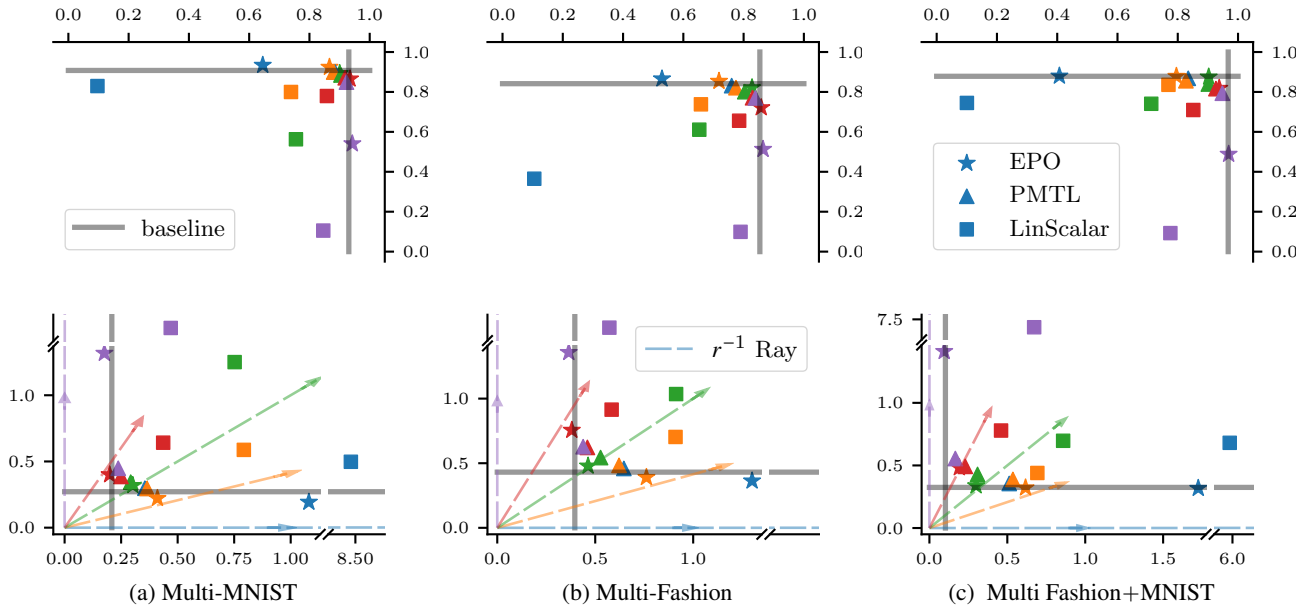

(a) Multi-MNIST (b) Multi-Fashion (c) Multi Fashion+MNIST

Figure 7. (Color Online) The top row show the accuracies, and the bottom row losses for 3 datasets. In each figure, x axis corresponds to task-1 while y axis corresponds to task-2. Different colors indicate different preference vectors, which are shown with corresponding r^{-1} rays. EPO solutions have the highest per-task accuracy and are closest to the preference vectors.

We run PMTL with the same reference vectors that are given as preferences to EPO search. The set of Pareto optimal solutions $\mathcal{P}$ for the multi-objective functions in (36) is a subset of the hyper-box $\mathcal{B} = \{\theta \in \mathbb{R}^n \mid -\mathbf{1}/\sqrt{n} \preccurlyeq_n \theta \preccurlyeq_n \mathbf{1}/\sqrt{n}\}$, where $\preccurlyeq_n$ denotes the partial ordering induced by the positive cone $\mathbb{R}^n_+$ in solution space. We test both the methods when initialization θ^0 is randomly sampled from inside and outside this hyper-box. PMTL is run for 200 iterations while EPO Search is run for only 80 iterations.

When initialization is inside the hyperbox (fig. 6, top row), we observe that PMTL, that does not use any uniformity-based criterion, descends in every step and reaches a Pareto optimal but not at the preference vectors. On the other hand, EPO search reaches the preference-specific solutions. When initialization is outside the hyperbox (fig. 6, bottom row), we see that EPO Search both descends and ascends in a controlled manner. It traces the Pareto front to find the required solutions, which makes it robust to initialization. No updates are seen in phase 2 of PMTL, when initialization is outside the hyper-box and far from the preference vectors. It reaches the Pareto front only in 2 out of 4 runs.

5.2. Real Data

Classification. We use three benchmark datasets: (1) MultiMNIST, (2) MultiFashion, and (3) Multi-Fashion+MNIST. In the MultiMNIST dataset (Sabour et al., 2017), two images of different digits are randomly picked from the original MNIST dataset (Lecun et al., 1998), and combined to form a new image, where one is in the top-left and the other is in the bottom-right. There is zero padding in the top-right and bottom-left. The MultiFashion dataset is generated in a similar manner from the FashionMNIST dataset (Xiao et al., 2017). In Multi-Fashion+MNIST dataset, one image is from MNIST (top-left) and the other image is from FashionMNIST (bottom-right). In each dataset, there are $120,000$ samples in the training set and $20,000$ samples in the test set. These are the same datasets used by Lin et al. (2019)[3].

For each dataset, there are two tasks: 1) classifying the top-left image, and 2) classifying the bottom-right image. Cross entropy losses are used for training. For a fair comparison with PMTL, we use the same network (LeNet (Lecun et al., 1998)) used in (Lin et al., 2019) as the MTL neural network. The baseline for comparison is training the network for individual tasks. In addition we show the results from linear scalarization (LinScalar). For all the methods stochastic gradient descent is used for training with the same hyperparameters: number of epochs, number of mini-batches and learning rate. We test the performance of all methods for the *same* 5 preference vectors, shown as rays in the bottom row of fig. 7. Ideal solutions should lie on these rays. Thus, each method has exactly 5 points corresponding to the test set losses in the bottom row and the top row shows the test set accuracies of the corresponding 5 DNN solutions.

The results in fig. 7. show that the per-task accuracy of

[3]Downloaded from: `https://github.com/Xi-L/ParetoMTL`

EPO search is higher than that of PMTL in every single run (top). The test set losses (bottom) show that the solutions from EPO search are closer to the corresponding preference vectors, compared to the solutions from PMTL.

We observe that the performance of LinScalar is worse than both the MOO-based methods. Recall that search direction is a convex combination of the gradients. In PMTL and EPO search, this combination is optimally chosen in each iteration. In LinScalar it is fixed, in every iteration, to the input user preference (L1 normalized). This causes opposing gradients to cancel each other and decrease the magnitude of the resulting update. Thus, update magnitude of LinScalar is lesser than that of other methods in almost every iteration. With learning rate and number of iterations fixed across methods, update magnitude finally determines proximity to the Pareto front.

Regression. We use the River Flow dataset (Spyromitros-Xioufis et al., 2016) that has $m = 8$ tasks: predicting the flow at 8 sites in the Mississippi River network. Each sample contains, for each site, the most recent and time-lagged flow measurements from $6, 12, 18, 24, 36, 48, 60$ hours in the past. Thus, there are 64 features and 8 target variables.

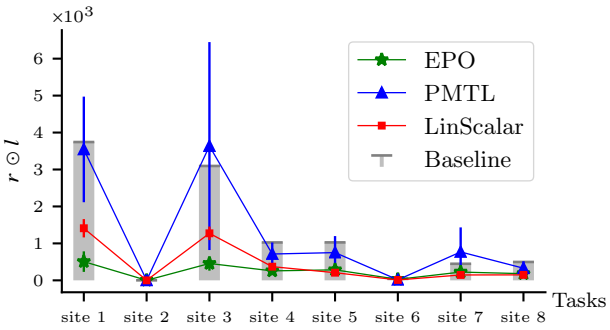

Figure 8. (Color Online) Comparison of mean RLP (with standard deviation; lower is better) of MTL methods after training the same neural network model to predict flow at 8 sites in the Mississippi River.

We remove samples with missing values and use $6,300$ samples for training and $2,700$ for testing. We use a fully connected feed-forward neural network (FNN) with 4 layers (layerwise sizes: $64 \to 32 \to 16 \to 8 \to 8$) with $n = 6,896$ parameters to fit the data. We randomly choose 20 input preference vectors $r \in \mathbb{R}^8_+$ (with $\sum_j r_j = 1$) and train the FNN using EPO search, PMTL and LinScalar. We use each of the 8 objectives trained separately as baselines. The same hyper-parameters are used for each method as done in the previous experiment. We used Mean Squared Error (MSE) as the loss for each task. Since visualization is difficult for 8 dimensions, we compare the methods using the relative loss profile (RLP) $r \odot l$ on the test data as shown in fig. 8.

We observe that EPO Search outperforms the other methods, indicating that it complies better with the input user preferences; the RLP of EPO search is more uniform (in the sense of definition (9)). Compared to the previous experiment with 2 tasks, the improvement over PMTL is higher. This is expected since the number of reference vectors required by PMTL, to reach a desired preference, grows exponentially with m. Interestingly, our method also improves over the baseline which shows the advantage of MTL for correlated tasks over learning each task independently: predicting river flow at one site helps improving the prediction at other sites as all the sites are from the same river.

Appendix C contains additional experimental results. We illustrate how EPO Search can trace the Pareto Front and scales with increasing number of objectives. We also evaluate EPO Search on a multi-label classification task.

6. Conclusion

EPO search advances the state-of-the-art in Multi-Objective Optimization and Multi-Task Learning. EPO Search finds the exact Pareto optimal solution for a given preference vector intersecting the Pareto front. We prove that for differentiable loss functions, it is guaranteed to converge. EPO search is robust to initialization and also provides a way to systematically traverse the Pareto front. This is achieved without compromising on scalability and EPO search can be used to train large-scale neural networks for MTL tasks, as seen in our experiments where EPO search outperforms competing approaches.

The combination of multiple gradient descent with controlled ascent makes EPO Search a unique approach that may find applications in other MOO problems. For instance, in *Interactive* MOO (Xin et al., 2018) where preference vectors are progressively varied until a satisfactory solution is obtained. In such cases, EPO Search that finds exact preference-specific solutions can be used as an effective tool for exploring the Pareto Front.

An exact Pareto optimal is also a preference-specific Pareto optimal solution, and thus EPO Search allows an MTL designer to find solutions with specific trade-offs or priorities among multiple tasks. Such preferences may be set based on task requirements or statistics of the data in each task. For example, data for tasks may differ in noise levels and practitioners can choose higher preferences for sources with less error. Thus, tasks with more accurate data will be fitted by the underlying DNN model better and this may avoid overfitting of noisy data. Another application could be in multi-class classification with imbalanced data. An effective approach in such cases is by re-weighting class-specific losses (Cui et al., 2019). This can be reformulated as a MTL problem, and solved using EPO Search, by considering the classification of each class as a task.

Acknowledgements

We thank the anonymous reviewers for their valuable feedback. VR was supported by the Singapore Ministry of Education Academic Research Fund [R-253-000-138-133].

References

GLPK (GNU linear programming kit). In *Linear Programming and Algorithms for Communication Networks*, pp. 25–29. CRC Press, aug 2012.

Bechikh, S., Kessentini, M., Said, L. B., and Ghédira, K. Preference incorporation in evolutionary multiobjective optimization: a survey of the state-of-the-art. In *Advances in Computers*, volume 98, pp. 141–207. Elsevier, 2015.

Boyd, S. and Vandenberghe, L. Vector optimization. In *Convex Optimization*, chapter 4.7, pp. 174–187. Cambridge University Press, 2004.

Caruana, R. Multitask learning. *Machine learning*, 28(1): 41–75, 1997.

Chen, Z., Badrinarayanan, V., Lee, C.-Y., and Rabinovich, A. Gradnorm: Gradient normalization for adaptive loss balancing in deep multitask networks. In *International Conference on Machine Learning (ICML)*, 2018.

Cheng, R., Jin, Y., Olhofer, M., and Sendhoff, B. A reference vector guided evolutionary algorithm for many-objective optimization. *IEEE Transactions on Evolutionary Computation*, 20(5):773–791, 2016.

Coello, C. C. Evolutionary multi-objective optimization: a historical view of the field. *IEEE Computational Intelligence*, 1(1):28–36, 2006.

Cohen, M. B., Lee, Y. T., and Song, Z. Solving linear programs in the current matrix multiplication time. In *Proceedings of the 51st annual ACM SIGACT symposium on theory of computing (STOC)*, pp. 938–942, 2019.

Cui, Y., Jia, M., Lin, T. Y., Song, Y., and Belongie, S. Class-balanced loss based on effective number of samples. *Proceedings of the IEEE Computer Society Conference on Computer Vision and Pattern Recognition*, 2019-June: 9260–9269, 2019.

Deb, K. *Multi-objective optimization using evolutionary algorithms*, volume 16. John Wiley & Sons, 2001.

Deb, K. Multi-objective optimization. In *Search methodologies*, pp. 403–449. Springer, 2014.

Deb, K. and Sundar, J. Reference point based multi-objective optimization using evolutionary algorithms. In *Proceedings of the 8th annual conference on Genetic and Evolutionary Computation*, pp. 635–642, 2006.

Désidéri, J. A. Multiple-gradient descent algorithm (MGDA) for multiobjective optimization. *Comptes Rendus Mathematique*, 2012.

Ehrgott, M. *Multicriteria optimization*, volume 491. Springer Science & Business Media, 2005.

Evtushenko, Y. G. and Posypkin, M. A deterministic algorithm for global multi-objective optimization. *Optimization Methods and Software*, 29(5):1005–1019, 2014.

Fliege, J. and Svaiter, B. F. Steepest descent methods for multicriteria optimization. *Mathematical Methods of Operations Research*, 51(3):479–494, 2000.

Fliege, J. and Vaz, A. I. F. A method for constrained multiobjective optimization based on sqp techniques. *SIAM Journal on Optimization*, 2016.

Fliege, J., Drummond, L. G., and Svaiter, B. F. Newton's method for multiobjective optimization. *SIAM Journal on Optimization*, 20(2):602–626, 2009.

Gandibleux, X. *Multiple criteria optimization: state of the art annotated bibliographic surveys*, volume 52. Springer Science & Business Media, 2006.

Heydari, A. A., Thompson, C. A., and Mehmood, A. Softadapt: Techniques for adaptive loss weighting of neural networks with multi-part loss functions. *arXiv preprint arXiv:1912.12355*, 2019.

Hillermeier, C. *Nonlinear multiobjective optimization: a generalized homotopy approach*, volume 135. Birkhaüser Verlag, 2001.

Lecun, Y., Bottou, L., Bengio, Y., and Haffner, P. Gradient-based learning applied to document recognition. *Proceedings of the IEEE*, 86(11):2278–2324, Nov 1998.

Lin, X., Zhen, H.-L., Li, Z., Zhang, Q.-F., and Kwong, S. Pareto multi-task learning. In *Advances in Neural Information Processing Systems (NeurIPS)*, pp. 12037–12047. 2019.

Liu, S., Johns, E., and Davison, A. J. End-to-end multi-task learning with attention. In *Proceedings of the IEEE Conference on Computer Vision and Pattern Recognition*, pp. 1871–1880, 2019a.

Liu, X., He, P., Chen, W., and Gao, J. Multi-task deep neural networks for natural language understanding. In *Proceedings of the 57th Annual Meeting of the Association for Computational Linguistics*, 2019b.

Marler, R. T. and Arora, J. S. Survey of multi-objective optimization methods for engineering. *Structural and multidisciplinary optimization*, 26(6):369–395, 2004.

Miettinen, K. *Nonlinear Multiobjective Optimization*. Springer, 1998.

Milojkovic, N., Antognini, D., Bergamin, G., Faltings, B., and Musat, C. Multi-gradient descent for multi-objective recommender systems. *arXiv preprint arXiv:2001.00846*, 2019.

Peitz, S. and Dellnitz, M. Gradient-based multiobjective optimization with uncertainties. In *NEO 2016*, pp. 159–182. Springer, 2018.

Rachmawati, L. and Srinivasan, D. Preference incorporation in multi-objective evolutionary algorithms: A survey. In *2006 IEEE International Conference on Evolutionary Computation*, pp. 962–968. IEEE, 2006.

Ramsundar, B., Kearnes, S., Riley, P., Webster, D., Konerding, D., and Pande, V. Massively multitask networks for drug discovery. *arXiv preprint arXiv:1502.02072*, 2015.

Ringkamp, M., Ober-Blöbaum, S., Dellnitz, M., and Schütze, O. Handling high-dimensional problems with multi-objective continuation methods via successive approximation of the tangent space. *Engineering Optimization*, 44(9):1117–1146, 2012.

Ruder, S. An overview of multi-task learning in deep neural networks. *arXiv preprint arXiv:1706.05098*, 2017.

Sabour, S., Frosst, N., and Hinton, G. E. Dynamic routing between capsules. In *Advances in Neural Information Processing Systems (NIPS)*, pp. 3856–3866. 2017.

Schütze, O., Dell'Aere, A., and Dellnitz, M. On continuation methods for the numerical treatment of multi-objective optimization problems. In *Dagstuhl Seminar Proceedings*. Schloss Dagstuhl-Leibniz-Zentrum für Informatik, 2005.

Sener, O. and Koltun, V. Multi-task learning as multi-objective optimization. In *Advances in Neural Information Processing Systems (NeurIPS)*, pp. 525–536. 2018.

Spyromitros-Xioufis, E., Tsoumakas, G., Groves, W., and Vlahavas, I. Multi-target regression via input space expansion: treating targets as inputs. *Machine Learning*, 104(1):55–98, 2016.

Steuer, R. E. The Tchebycheff procedure of interactive multiple objective programming. In Karpak, B. and Zionts, S. (eds.), *Multiple Criteria Decision Making and Risk Analysis Using Microcomputers*. Springer, 1989.

Trohidis, K., Tsoumakas, G., Kalliris, G., and Vlahavas, I. Multi-label classification of music by emotion. *EURASIP Journal on Audio, Speech, and Music Processing*, 2011 (1):4, 2011. ISSN 1687-4722.

Wang, P., Yang, R., Cao, B., Xu, W., and Lin, Y. Dels-3d: Deep localization and segmentation with a 3d semantic map. In *Proceedings of the IEEE Conference on Computer Vision and Pattern Recognition*, pp. 5860–5869, 2018.

Wiecek, M. M., Ehrgott, M., and Engau, A. *Continuous Multiobjective Programming*. Springer, 2016.

Xiao, H., Rasul, K., and Vollgraf, R. Fashion-mnist: a novel image dataset for benchmarking machine learning algorithms. *CoRR*, abs/1708.07747, 2017.

Xin, B., Chen, L., Chen, J., Ishibuchi, H., Hirota, K., and Liu, B. Interactive multiobjective optimization: A review of the state-of-the-art. *IEEE Access*, 6:41256–41279, 2018.

Zerbinati, A., Desideri, J.-A., and Duvigneau, R. Comparison between MGDA and PAES for multi-objective optimization. *Research Report, INRIA*, RR-7667, 2011.

Zhang, B., Provost, E. M., and Essl, G. Cross-corpus acoustic emotion recognition with multi-task learning: Seeking common ground while preserving differences. *IEEE Transactions on Affective Computing*, 10(1):85–99, 2017.

Zhang, Q., Zhou, A., and Jin, Y. RM-MEDA: A regularity model-based multiobjective estimation of distribution algorithm. *IEEE Transactions on Evolutionary Computation*, 12(1):41–63, 2008.

Zhang, Y. and Yang, Q. An overview of multi-task learning. *National Science Review*, 5(1):30–43, 2018.